Journal of Taibah University for Science

ISSN: (Print) (Online) Journal homepage: www.tandfonline.com/journals/tusc20

Mechanical and biological evaluation of β-dicalcium silicate/dicalcium phosphate-based cements: promising materials for biomedical applications

Ammar Z. Alshemary, Almataz Bellah Marandi, Daver Ali, Tuğba Köse, Ali Deniz Dalgic, Ali Motameni & Zafer Evis

To cite this article: Ammar Z. Alshemary, Almataz Bellah Marandi, Daver Ali, Tuğba Köse, Ali Deniz Dalgic, Ali Motameni & Zafer Evis (2025) Mechanical and biological evaluation of β-dicalcium silicate/dicalcium phosphate-based cements: promising materials for biomedical applications, Journal of Taibah University for Science, 19:1, 2461817, DOI: 10.1080/16583655.2025.2461817

To link to this article: https://doi.org/10.1080/16583655.2025.2461817

JOURNAL OF TAIBAH UNIVERSITY FOR SCIENCE
2025, VOL. 19, NO. 1, 2461817
https://doi.org/10.1080/16583655.2025.2461817

Mechanical and biological evaluation of β-dicalcium silicate/dicalcium phosphate-based cements: promising materials for biomedical applications

Ammar Z. Alshemary [a,b,c], Almataz Bellah Marandi [d], Daver Ali [d], Tuğba Köse [e], Ali Deniz Dalgic [e], Ali Motameni [f] and Zafer Evis [g]

[a]Nanomaterials Research Center, Department of Chemistry, College of Science, Mathematics and Technology, Wenzhou-Kean University, Wenzhou, People's Republic of China; [b]Dorothy and George Hennings College of Science, Mathematics and Technology, Kean University, Union, NJ, USA; [c]Zhejiang Bioinformatics International Science and Technology Cooperation Center, Wenzhou, People's Republic of China; [d]Faculty of Engineering, Department of Biomedical Engineering, Karabuk University, Karabuk, Turkey; [e]Department of Genetics and Bioengineering, Istanbul Bilgi University, Istanbul, Turkey; [f]Department of Metallurgical and Materials Engineering, Middle East Technical University, Ankara, Turkey; [g]Engineering Sciences, Middle East Technical University, Ankara, Turkey

ABSTRACT
This study explores the synthesis and evaluation of β-Dicalcium silicate and Dicalcium phosphate-based cements for biomedical use. β-Tricalcium phosphate was synthesized using microwave-assisted wet precipitation, while β-Dicalcium silicate was prepared via the sol-gel method. Composites with varying β-Dicalcium silicate contents (20%, 30%, 40%) were formulated and characterized using X-ray diffraction, Fourier-transform infrared spectroscopy, and Field emission scanning electron microscope analyses. The 40% β-Dicalcium silicate composite showed the highest compressive strength at 10.22 MPa. Antibacterial tests against *Staphylococcus aureus* revealed that gentamicin-loaded Dicalcium phosphate cement had superior properties. Cytotoxicity studies using the Osteogenic sarcoma cell line revealed that the β-Dicalcium Silicate /Dicalcium Phosphate composites supported better cell viability compared to pure Dicalcium phosphate cement, with the 20% β-Dicalcium silicate /Dicalcium phosphate composition being the most effective in promoting cell growth. These findings suggest that β-Dicalcium silicate /Dicalcium phosphate composites hold promise for biomedical applications.

ARTICLE HISTORY
Received 4 October 2024
Revised 6 January 2025
Accepted 29 January 2025

KEYWORDS
Biocements; dicalcium phosphate; β-dicalcium silicate; antibacterial activity; compressive strength; cytotoxicity

Highlights

- β-TCP synthesized via microwave-assisted wet precipitation; $\beta-C_2Si$ prepared using the sol–gel method.
- β-TCP particles have been used to prepare DCP cements and β-C_2S particles have been used as dopants.
- XRD, FTIR, and FESEM techniques confirmed phase purity and structural properties.
- Compressive stress improved with increasing $\beta-C_2Si$ content, peaking at 10.22 MPa for the 40% $\beta-C_2Si$/DCP composite.
- Pure DCP cement loaded with gentamicin showed superior antibacterial properties, especially at 0.2 g/mL concentration.
- $\beta-C_2Si$/DCP composites supported better cell viability compared to pure DCP cement, with the 20% $\beta-C_2Si$/DCP composition being the most effective in promoting cell growth.

1. Introduction

Dicalcium phosphate (DCP) cements have been widely studied for bone repair and regeneration applications. These materials are known for their excellent biocompatibility, bioactivity, and osteoconductive properties [1]. DCP cement has shown promise in promoting bone formation and integration with the host tissue. Studies have demonstrated that DCP can support cell attachment, proliferation, and differentiation, making it a suitable candidate for bone repair applications [2].

However, these materials suffer from poor mechanical properties, which limit their use in load-bearing applications. DCP cements often exhibit low tensile and flexural strengths [3–5], significantly lower than natural bone ones. To address these limitations, researchers have explored several strategies to enhance the mechanical properties of DCP-based cements. One approach involves incorporating polymer additives, such as PEGylated poly(glycerol-sebacate) (PEGS), which has been shown to improve the compressive

CONTACT Ammar Z. Alshemary aalshema@kean.edu Nanomaterials Research Center, Department of Chemistry, College of Science, Mathematics and Technology, Wenzhou-Kean University, 88 Daxue Road, Ouhai, Wenzhou 325060, Zhejiang Province, People's Republic of China; Dorothy and George Hennings College of Science, Mathematics and Technology, Kean University, 1000 Morris Ave, Union, NJ 07083, USA; Zhejiang Bioinformatics International Science and Technology Cooperation Center, Ouhai, Wenzhou, 325060 Zhejiang Province, People's Republic of China

strength of calcium phosphate cements by creating a more cohesive and less porous structure [6]. Another strategy is the reinforcement of DCP cements with short-length fibres, such as polyhydroxyalkanoate (PHA) fibres, which enhance the elasticity and mechanical strength of the cements [7]. These fibres help to distribute stress more evenly throughout the material, reducing the likelihood of fracture. The incorporation of nanoparticles, such as graphene oxide or strontium nitrate, has also been investigated as a means to improve the mechanical properties of DCP cements. Graphene oxide-reinforced DCP cements have demonstrated enhanced mechanical properties and increased adsorption capacity, which can contribute to better overall performance in bone tissue regeneration [8]. Similarly, strontium nitrate doping has been shown to significantly improve the compressive strength and mechanical performance of DCP cements, making them more suitable for load-bearing applications [9]. Optimizing the particle size and distribution of the cement components can also lead to improved packing density and enhanced mechanical properties [10,11]. Furthermore, other chemical additives, such as citric acid or sodium citrate, can modify the setting reaction and crystal formation, resulting in stronger cements [12].

β-Dicalcium Silicate (β-C_2Si), a calcium silicate compound, has emerged as a promising additive for biomedical applications, particularly in bone repair and regeneration, due to its excellent mechanical properties and bioactivity [13]. Among the various techniques used to prepare β-C_2Si, the sol–gel method offers several advantages for producing bioactive cement composites. This process allows for precise control over composition and nanostructure through molecular-level mixing of liquid precursors [14,15]. Key steps in the sol–gel synthesis typically include preparing calcium and silicon precursor solutions, hydrolysis and condensation reactions to form a sol, gelation to create a three-dimensional network, aging and drying to remove solvents, and heat treatment to obtain the final crystalline β-C_2Si phase. The method enables low-temperature processing compared to traditional solid-state reactions, helping maintain phase purity and providing control over particle size, porosity, and surface area, which are crucial for the cement's reactivity and mechanical properties [14,15]. Common challenges in sol–gel synthesis of calcium silicates include controlling hydrolysis and condensation rates, preventing premature calcium precipitation, optimizing drying conditions, and achieving complete conversion to β-C_2Si during heat treatment. Researchers typically employ X-ray diffraction, FTIR spectroscopy, and scanning electron microscopy to confirm the successful production of β-C_2Si with the desired phase purity and structural characteristics [14,16]. The sol–gel process contributes to producing homogeneous, high-purity β-C_2Si with controlled nanostructure suitable for biomedical applications.

Studies have demonstrated that incorporating β-C_2Si into cement matrices can enhance the mechanical properties of composite materials, improve compressive strength, and promote cell viability and proliferatio [13,17]. Incorporating β-C_2Si into cement matrices has been reported to improve compressive strength and support better cell viability than pure cement formulations. The incorporation of β-C_2Si into DCP cements aims to leverage the benefits of both materials, potentially creating a composite with enhanced mechanical properties, improved bioactivity, and maintained biocompatibility [14]. Incorporating antibiotics into calcium phosphate-based cements is a common strategy to enhance their antibacterial properties [18,19]. While specific studies on β-C_2Si/DCP composites loaded with antibiotics are limited, research on similar calcium phosphate cements has shown that antibiotic-loaded formulations can effectively inhibit bacterial growth and reduce the risk of infection at the implantation site.

A key aspect of the study's originality is the formulation of various β-C_2Si/DCP cement composites with different β-C_2Si contents (20%, 30%, and 40%), which demonstrated enhanced mechanical properties, particularly improved compressive strength with increasing β-C_2Si content. The investigation also provides novel insights into the antibacterial activity of these composites against *Staphylococcus aureus* (*S. aureus*) and their cytocompatibility using Osteogenic sarcoma (Saos-2) cells, revealing that β-C_2Si/DCP composites support better cell viability compared to pure DCP cement. Furthermore, the study identifies optimal pH conditions for cell proliferation, contributing valuable knowledge to the field of biomedical materials. By combining these elements, the research offers a comprehensive understanding of the structural, mechanical, and biological properties of these novel cement composites, paving the way for their potential use in advanced biomedical applications.

2. Materials and methods

Calcium nitrate tetrahydrate ($Ca(NO_3)_2{\cdot}4H_2O$), diammonium hydrogen phosphate ($(NH_4)_2HPO_4$), and tetraethyl orthosilicate (TEOS, $Si(OC_2H_5)_4$) were used as sources of Ca^{2+}, $PO_4{}^{3+}$, and SiO_2, respectively, to prepare β-TCP/β-C_2Si composite materials. Monocalcium phosphate monohydrate (MCPM, $Ca(H_2PO_4)\ {}_2{\cdot}H_2O$) was used as a precursor to prepare DCP cements. Ammonium hydroxide (NH_4OH) was used in this study to adjust the pH value. All materials were purchased from Merck, Germany.

2.1. Synthesis of β-TCP powder

The β-TCP material was produced by microwave-assisted wet precipitation [20]. For Solution (A), 42.51 grams of $Ca(NO_3)_2{\cdot}4H_2O$ were dissolved in 200 mL of distilled H_2O. Solution (B) was prepared by dissolving 15.85 g $(NH_4)_2HPO_4$ in 200 mL of distilled H_2O. Solution (B) was progressively added to Solution (A) while stirring. NH_4OH was added to adjust the solution's pH to 7. After 30 minutes of stirring at room temperature, the mixture was microwaved for 5 minutes at 800 watts in a SAMSUNG MS23F301EAW microwave oven. The product was then filtered and rinsed with distilled H_2O. The sample was dried overnight at 80°C in an oven. Finally, the resulting white powder was heat-treated at 1000°C for 2 h.

2.2. Synthesis of β-C_2Si powder

β-C_2Si was synthesized using the sol–gel technique with a calcium-to-silicon (Ca/Si) molar ratio 1.4:1 [21]. The synthesis was initiated by dissolving 83.6 mL of TEOS in a mixture of ethanol (314.6 mL) and distilled water (45 mL). After 30 minutes of agitation, 0.5 mL of acetic acid was added as a catalyst to initiate TEOS hydrolysis. The solution was stirred at ambient temperature overnight to ensure complete hydrolysis, followed by adding 119.27 g of $Ca(NO_3)_2 \cdot 4H_2O$. This mixture was stirred at 60°C for 6 h and then left at room temperature for 24 h to allow gelation. The resulting hydrogel was dehydrated at 80°C for 48 h, followed by calcination at 800°C with a heating rate of 10°C/min for 3 h [14,21].

2.3. Synthesis of pure DCP and β-C_2Si/DCP cement composites

The pure phase of DCP cement was prepared by mixing 1.0 g of β-TCP and 0.5 g of MCPM powders in a mortar. Precisely 0.8 mL of distilled H_2O was then added to the powder mixture and vigorously mixed until a homogenous paste was achieved, which subsequently self-hardened at room temperature. The β-C_2Si/DCP cement composites were prepared using a similar protocol. Various amounts of β-C_2Si powder were combined with β-TCP and MCPM powders. The mixture was thoroughly blended, and a suitable amount of water was added at a ratio of 0.8 mL per 1 gram of powder. Different β-C_2Si/DCP cement composites were prepared, as summarized in Table 1.

2.4. Microstructural characterizations

The phase purity of the synthesized materials was determined using an X-ray diffractometer (XRD, Rigaku Ultima IV). The scan angles ranged from 20° to 80°. Lattice parameters and crystallinity were analyzed. Fourier Transform Infrared Spectroscopy (FTIR, Bruker IFS66/S) identified the functional group vibration modes in the powdered samples. Particle morphology was examined with a Field Emission Scanning Electron Microscope (FESEM, Quanta 400F), and the average particle size was measured using ImageJ software. Thermogravimetric analysis (TGA, PerkinElmer Pyris 1) was conducted in a nitrogen atmosphere from room temperature to 950°C to evaluate the thermal stability of the materials.

Table 1. Various compositions of pure DCP and β-C_2Si/DCP cement composites.

	Solid Phase (g)			Liquid Phase (mL)
Sample ID	β-TCP	MCPM	β-C_2Si	H_2O
Pure DCP	1.00	0.50	0.00	0.80
20% β-C_2Si/DCP	1.00	0.50	0.30	0.95
30% β-C_2Si/DCP	1.00	0.50	0.45	1.03
40% β-C_2Si/DCP	1.00	0.50	0.60	1.10

2.5. Compressive strength test

To prepare standardized cement paste samples, cylindrical moulds with internal dimensions of 6 mm diameter and 12 mm height were utilized, in accordance with ASTM F451-15 specifications. Following self-hardening at lab temperature, the cement specimens were carefully extracted from the moulds. Compressive strength testing was conducted using a Universal Instron testing machine. The samples were subjected to a constant crosshead speed of 4 mm/min until failure occurred. To ensure reliability and statistical significance, the tests were performed in triplicate for each cement formulation.

2.6. Loading of antibiotic

Gentamicin sulphate (Merck, Germany) was used as an antibiotic drug. Approximately 2 mg of the drug was dissolved in 1 mL of distilled water to create a stock solution. This drug solution was then used as the liquid phase for the preparation of cement samples. The drug-loaded cement samples were prepared for subsequent evaluation of antibacterial properties and cell culture analysis.

2.7. In Vitro antibacterial activity

Broth microdilution method was used to determine antimicrobial efficacy of drug-loaded cement samples against selected bacterial strains [22]. Drug-loaded cement extracts were prepared by following ISO 10993 standards for biomaterial testing with a recommended concentration of 0.2 g/mL in sterilized Lysogeny broth (LB) media. The extracts were incubated for 24 h at 37 °C, then sterilized by a 0.22 μm pore-sized filter. The serial dilutions (0.2, 0.1, 0.05, 0.025, 0.0125, and 0.00625 g/mL) were prepared from the extract with an initial 0.2 g/mL concentration in 96 well plates. Staphylococcus aureus (*S. aureus*, gram-positive, ATCC 6538) was cultured overnight at 37°C following the aseptic technique requirements. For the optical density (OD) control, the overnight culture of *S. aureus* was sub-cultured, and the OD600 values were measured hourly. 10 µl of *S. aureus* samples (OD600 = 0.4) were inoculated in 96 well plates with the extracts. The OD600 measurements were repeated at 0 h and 24 h with the microplate reader.

2.8. In Vitro cell culture studies

The effect of drug-loaded cements on Osteogenic sarcoma (Saos-2) cell line viability was evaluated using Osteogenic sarcoma Deep Blue assay. Soas-2 cells were cultured in Dulbecco's MEM (DMEM; Merk Germany) containing 10% heat-inactivated fetal bovine serum (FBS) and 1% penicillin/streptomycin (Invitrogen, USA) at 37°C in a 5% CO_2 containing environment. The compressed discs of the samples were UV sterilized, and discs were placed in a 24 well plate containing DMEM and incubated for 24 h. After the incubation, the media was discarded, and 1 × 10^4 Saos-2 cells were seeded in a 20 µL drop-on disc sample. After 2 h of incubation for the cells to attach, the medium was completed to 100 µL to cover the disc surfaces, and the plate was incubated at 37 °C. Deep Blue reagent was added to each well to obtain a 10% final concentration, and the plate was incubated for 4 h. After incubation, Deep Blue reagent-containing media was transferred into a new 24-well plate for fluorescence measurement. Since the deep blue reagent does not harm the cells, Saos-2 cells continued to grow by adding the fresh medium after removing the deep blue reagent-containing media. A microplate reader (Varioskan Flash Spectral Scanning Multimode Reader, Thermo Scientific) was used for the 530–590 nm fluorescence measurement for excitation and emission respectively. The measurements were repeated on day 1, day 4, and day 7.

2.9. Statical analysis

Statistical analyses were conducted using IBM SPSS Statistics version 22.0. To compare mean values between groups and assess the statistical significance of observed differences, one-way analyses of variance and post hoc Tukey tests for multiple comparisons were performed. Differences were considered statistically significant when the *p*-value was less than 0.05.

3. Results and discussion

3.1. Structural characterization of β-TCP and β-C_2Si powders

Figure 1(a) illustrates the diffraction pattern seen in β-TCP powder. The diffraction peaks seen in the synthesized β-TCP were very similar to those seen in the standard β-TCP phase (whitlockite phase, JCPDS 09–0169) [23]. The analysis detected no additional calcium phosphate phases. In particular, the analysis showed no clear peak at 32.196°. This meant that the powder that was made was uniform and did not contain the hydroxyapatite phase (HA, JCPDS 09–432). Figure 1 (b) represents the FTIR spectrum of β-TCP powder. The peaks around 1040 cm^{-1} and 1090 cm^{-1} correspond to the asymmetric stretching vibrations of the $PO_4{}^{3+}$ ($\upsilon3$) group. These vibrations are typically strong and are a characteristic feature of phosphate compounds. The peak around 960 cm^{-1} is attributed to the symmetric stretching mode of the $PO_4{}^{3+}$ ($\upsilon1$) group. The peaks around 600 cm^{-1} and 560 cm^{-1} are associated with the bending vibrations of the $PO_4{}^{3+}$ ($\upsilon4$) group. This peak is due to the stretching vibrations of the carbonate groups, which may be present as impurities or as a result of partial substitution in the crystal lattice of β-TCP [24]. The presence of strong peaks corresponding to the ν_3, ν_1, and ν_4 vibrations of the phosphate groups confirms the characteristic structure of β-TCP, which is primarily composed of phosphate units. The peaks around 1200 cm^{-1} and 900 cm^{-1} are attributed to the $P_2O_7{}^{4-}$ groups, which are pyrophosphate groups, indicating that some degree of substitution or secondary phases might be present in the β-TCP sample [25]. The peaks observed around 1723cm^{-1} indicate the presence of carbonate groups (C = O). This is common in calcium phosphate materials, as they can easily incorporate carbonate ions from the environment [24]. Figure 1 (c) represents particles in the SEM image, and several particles appear as thin, flat plates with sharp edges. The particles do not have uniform shapes and sizes, indicating a semi-spherical, irregular morphology typical of β-TCP. The particles vary in size, with many appearing to be in the range of a few micrometers. Some larger particles are approximately 10 µm in length, while smaller fragments are less than 1 µm. The Ca/P ratio was also determined to be 1.39, slightly lower than the desired value of 1.5.

Figure 2 (a) represents the XRD pattern of β-C_2Si powder that was prepared using the sol–gel method. The observed patterns correspond to the confirmed diffraction data for β-C_2Si (PDF#33-0302). Contaminants like calcium oxide (CaO) and silicon dioxide (SiO_2) were absent from the powders generated. The synthesized C_2Si exhibited significant crystallinity, as shown by the sharp and narrow diffraction peaks. Figure 2 (b) represents the FTIR spectrum of β-C_2Si structure. Two peaks located at $\sim$3400 cm^{-1} and $\sim$1600 cm^{-1} which could be attributed to the O-H stretching and bending vibrations of water molecules, respectively. These peaks indicate that the sample contains water, likely as adsorbed moisture or structural water. Another peak was detected at $\sim$1450 cm^{-1}. This peak corresponds to the asymmetric stretching vibration of the carbonate ion ($CO_3 \supset 2^-$). This peak suggests that the sample may contain some carbonate impurities or has undergone carbonation.

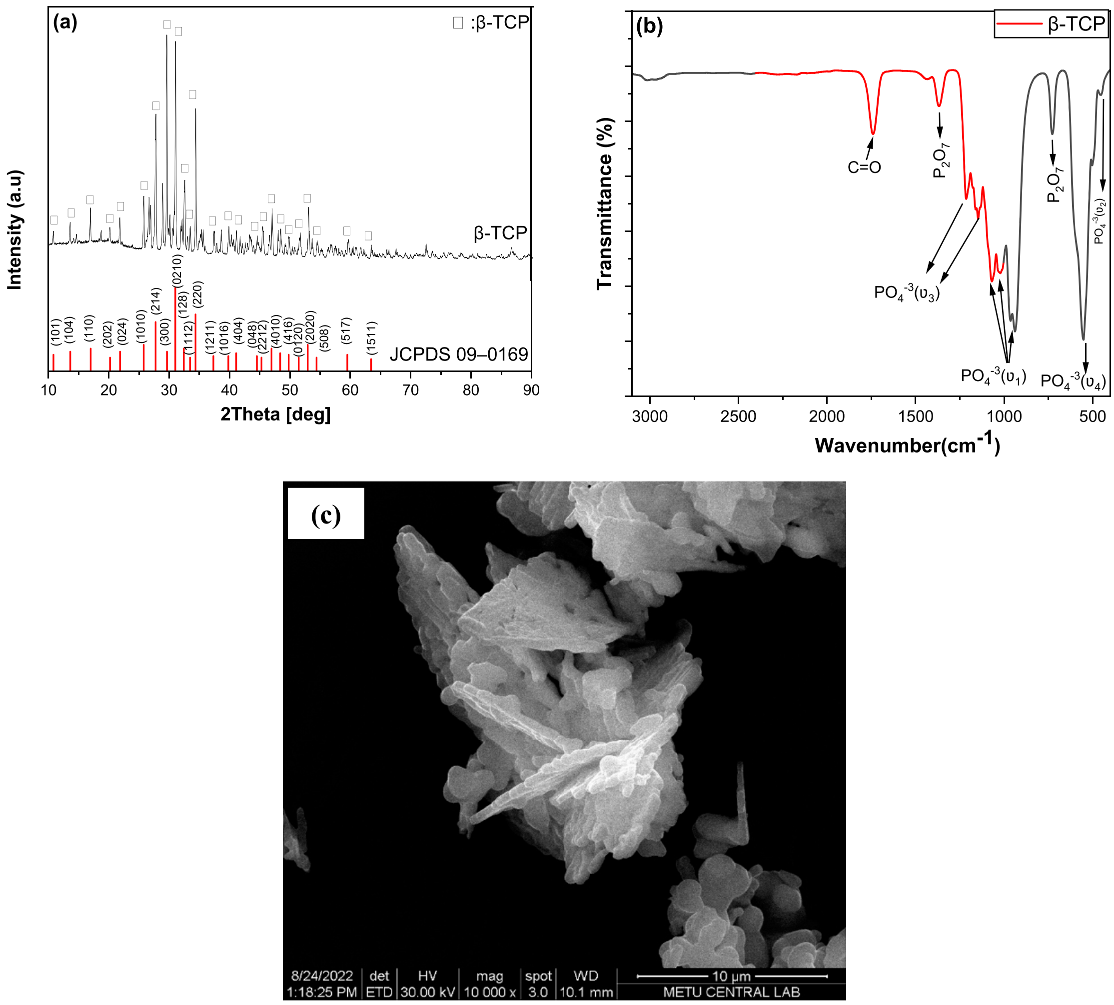

Figure 1. (a) XRD pattern, (b) FTIR spectrum and (c) FESEM image of β-TCP powders.

Furthermore, big peaks were observed at $\sim 1000\,cm^{-1}$ and $\sim 500\,cm^{-1}$. These peaks are characteristic of the stretching and bending vibrations of the silicate tetrahedra (SiO_4^{4-}). The strong peak around $1000\,cm^{-1}$ is typically associated with the Si-O stretching vibrations, while the peak around $500\,cm^{-1}$ is due to the Si-O bending vibrations. The β-C_2Si specific peaks around $\sim$900-1100 cm^{-1}. This region shows multiple peaks that are characteristic of β-C_2Si. These peaks arise from the complex vibrational modes of the silicate framework in the β-C_2Si structure. Figure 2(c) represents the SEM image of β-C_2Si, showing a rough, porous surface with irregular shapes and textures. This morphology is typical of β-C_2Si, which can contribute to its reactivity in cementitious applications. The particles appear in the micrometer range, consistent with the scale bar provided. The image reveals a high degree of porosity, which is common for β-C_2Si and can affect its hydration properties and strength development in cement.

3.2. Microstructure and biological properties of pure DCP and β-C_2Si/DCP cement composites

Figure 3 presents the XRD patterns of pure DCP and β-C_2Si/DCP cements self-hardened at room temperature. The XRD peaks revealed the highest levels of intensity at 2θ values of 20.95°, 29.2°, 30.6°, 34.1°, and 34.3°. The prepared pure DCP agreed well with the brushite phase (JCPDS 09-0077). With the incorporation of β-C_2Si into DCP cements, alterations in the intensity and morphology of the peaks were apparent. The addition of 20% β-C_2Si reduces peak intensity compared to pure DCP, suggesting a decrease in crystallinity [26]. With 30% β-C_2Si, the peaks become broader and less intense, indicating reduced crystallinity and smaller particle size. At 40% β-C_2Si, the peaks are even broader and less intense, confirming the trend of decreasing crystallinity and particle size with increasing β-C_2Si content [27]. The diffraction peaks shift to the left (lower 2θ angles) with increasing β-C_2Si content. This effect could be attributed to the leaching of silicon (Si) from β-C_2Si and its subsequent incorporation into the DCP structure, causing a left shift in the diffraction pattern. The observed shift could be due to the replacement of phosphate ions by silicate ions within the crystal lattice. The silicate ion (0.39 Å) has a larger ionic radius compared to the phosphate ion (0.35 Å). Consequently, at high concentrations, the substitution of phosphate ions in DCP by silicate ions would be expected to further increase the lattice parameters, resulting in a left shift of

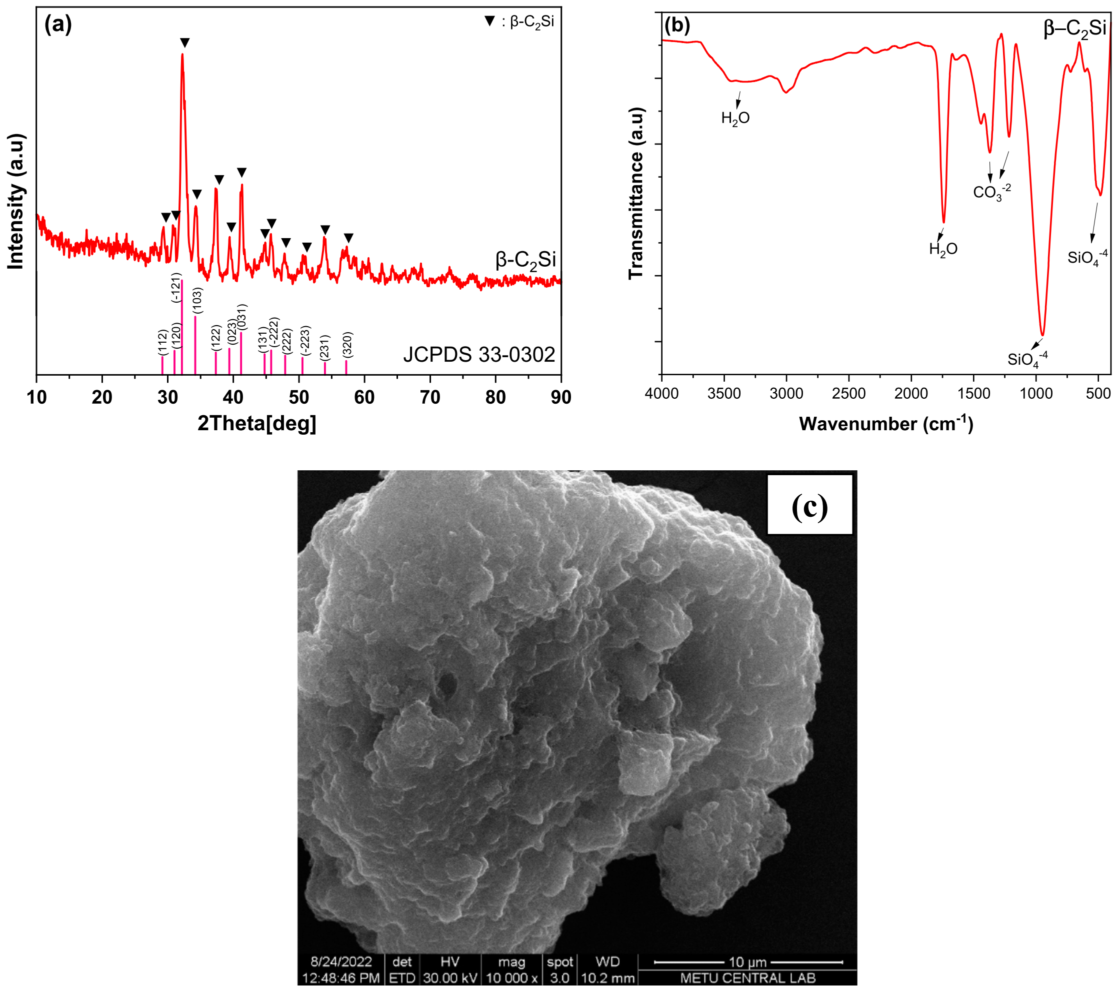

Figure 2. (a) XRD pattern, (b) FTIR spectrum and (c) FESEM image of β-C_2Si powders.

the diffraction peaks [28,29]. The decrease in peak intensity and increase in peak broadening with higher β-C_2Si content suggests that the crystallinity of the composite materials decreases as more β-C_2Si is added. The broadening of the peaks indicates a reduction in particle size, consistent with the formation of smaller crystallites or more amorphous material. The XRD patterns provide clear evidence that the addition of β-C_2Si to DCP affects the crystallinity, particle size, and lattice parameters of the resulting composite materials.

Figure 4 represents the FTIR spectra of DCP combined with different fractions of β-C_2Si. Three peaks at 1213 cm^{-1}, 1128 cm^{-1}, and 1058 cm^{-1} can be seen, which could be attributed to $P = O$ stretching. Another three peaks located at 986 cm^{-1}, 873 cm^{-1}, and 789 cm^{-1} are assigned to P-O-P stretching. Additionally, three peaks detected at 656 cm^{-1}, 574 cm^{-1}, and 519 cm^{-1} are due to P-O stretching. Besides the phosphate peaks, a peak was observed at 1649 cm^{-1}, attributed to O-H bending belonging to the H_2O molecule. The presence of water molecules indicates that the structure of the cement is in the brushite phase ($CaHPO_4{\cdot}2H_2O$), which is in good agreement with the XRD results (Figure 3). With the incorporation of 20% β-C_2Si into DCP, the peak areas of P-O-P and $P = O$ stretching increased, and the peaks became broader, possibly due to overlapping with the $SiO_4{}^{4-}$ stretching group. Another peak was also detected at 1370 cm^{-1}, attributed to $CO_3{\supset}2^-$ stretching, suggesting carbonate contamination or formation. With increasing amounts of β-C_2Si to 30% and 40%, similar peaks to the 20% β-C_2Si/DCP sample were observed but with increased intensity. This indicates a higher concentration of silicate and carbonate groups, showing a higher incorporation of β-C_2Si into the DCP matrix. The characteristic $P = O$, P-O-P, and P-O peaks of DCP are present in all samples but show variations in intensity and position due to the doping effect. The changes in the phosphate-related peaks reflect the structural modifications in the DCP due to the incorporation of β-C_2Si.

Figure 5 depicts the microstructure of pure DCP cement and β-C_2Si/DCP composite cement. The FESEM analysis revealed distinct characteristics of the particles in each material. Pure DCP particles exhibited a non-symmetrical plate-like structure, with average widths ranging from micro to nanometre dimensions. Variations in plate diameters were attributed to differing agglomeration levels. In contrast, adding 20% β-C_2Si resulted in a highly cross-linked structure. This modification was characterized by the development of a

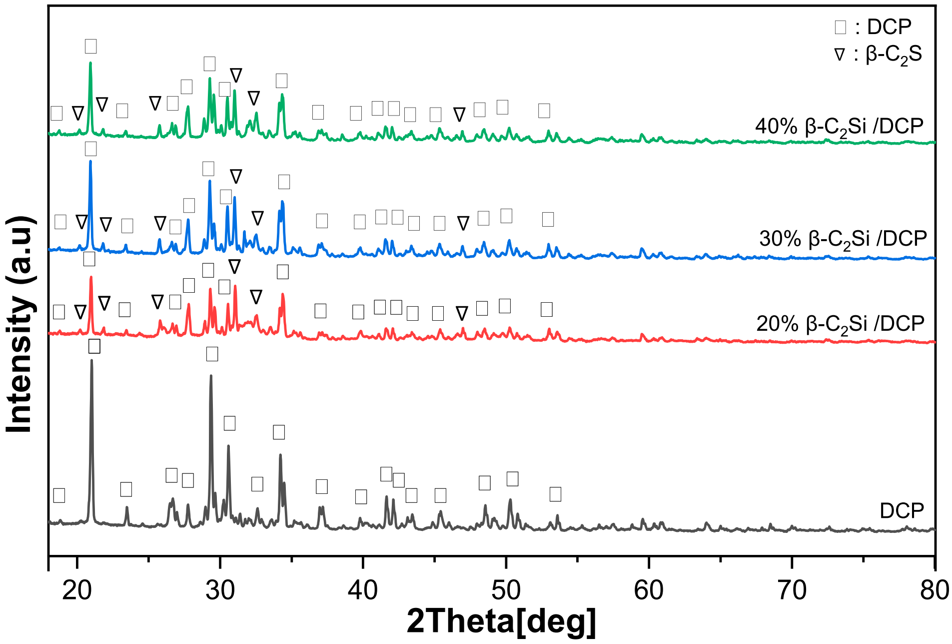

Figure 3. XRD patterns of pure DCP and β-C_2Si/DCP cement composite.

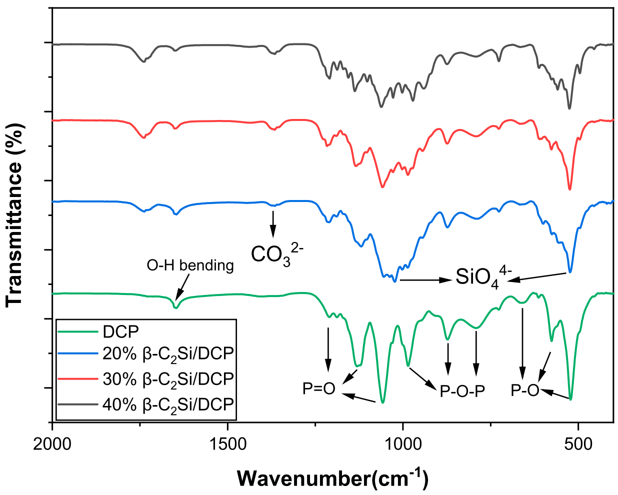

Figure 4. FTIR patterns of pure DCP and β-C_2Si / DCP cement composites.

fibrous surface on the cement particles and the presence of minor pore formations. As the proportion of β-C_2Si increased to 40%, the microstructure showed a notable shift. Plate-like particles became more prominent and exhibited a slightly spherical shape, indicative of a more homogeneous distribution within the cement matrix. These findings show that β-C_2Si changes the microstructural properties of the cement and emphasizes its role in changing the shape and distribution of the particles.

The thermal stability of pure DCP cement and β-C_2Si/DCP cement composites is illustrated in Figure 6. Three distinct stages of weight loss in pure DCP cement occur within the temperature ranges of 30-190°C, 190-450°C, and 450-700°C. The initial stage, from 30 to 190°C, primarily involves the removal of residual moisture and the H_2O molecules from DCP (brushite, $CaHPO_4{\cdot}2H_2O$) cement, converting it to the monetite phase ($CaHPO_4$) [30]. In the subsequent stage, between 190 and 450°C, the decomposition of $CaHPO_4$ occurs, eliminating water molecules and forming calcium pyrophosphate (γ-$Ca_2P_2O_7$) (Eq. 1) [31,32], as described by the equation:

$$2CaHPO_4 \rightarrow Ca_2P_2O_7 + H_2O \qquad (1)$$

The third stage, occurring between 450 and 700°C, involves further transformations. Calcium pyrophosphate may transform into other phases as the temperature increases. At temperatures around 600°C, γ-$Ca_2P_2O_7$ probably transformed to β-$Ca_2P_2O_7$ [33]. Above 700°C, there is negligible further weight reduction, indicating that the samples stabilize after calcination beyond this temperature threshold, consistent with observations at 800°C. Incorporating β-C_2Si into the cement mixture resulted in a lower rate of weight loss. Additionally, all samples exhibited thermal stability at temperatures of 700°C and higher. Notably, the TGA curve for the 20% β-C_2Si/DCP sample displayed elevated humidity levels. The respective weight loss percentages for pure DCP, 20% β-C_2Si/DCP, 30% β-C_2Si/DCP, and 40% β-C_2Si/DCP were 21.2%, 17.4%, 11.6%, and 15.9%.

The thermal stability of the prepared cement composites is clearly improved with the incorporation of β-C_2Si. This can be attributed to β-C_2Si having a stable crystal structure that remains intact at high temperatures. This stability is crucial for maintaining the integrity of the cement matrix when exposed to thermal stress [34]. Additionally, when β-C_2Si hydrates, it forms calcium silicate hydrate (C–S–H), which contributes to the mechanical strength and thermal stability of the

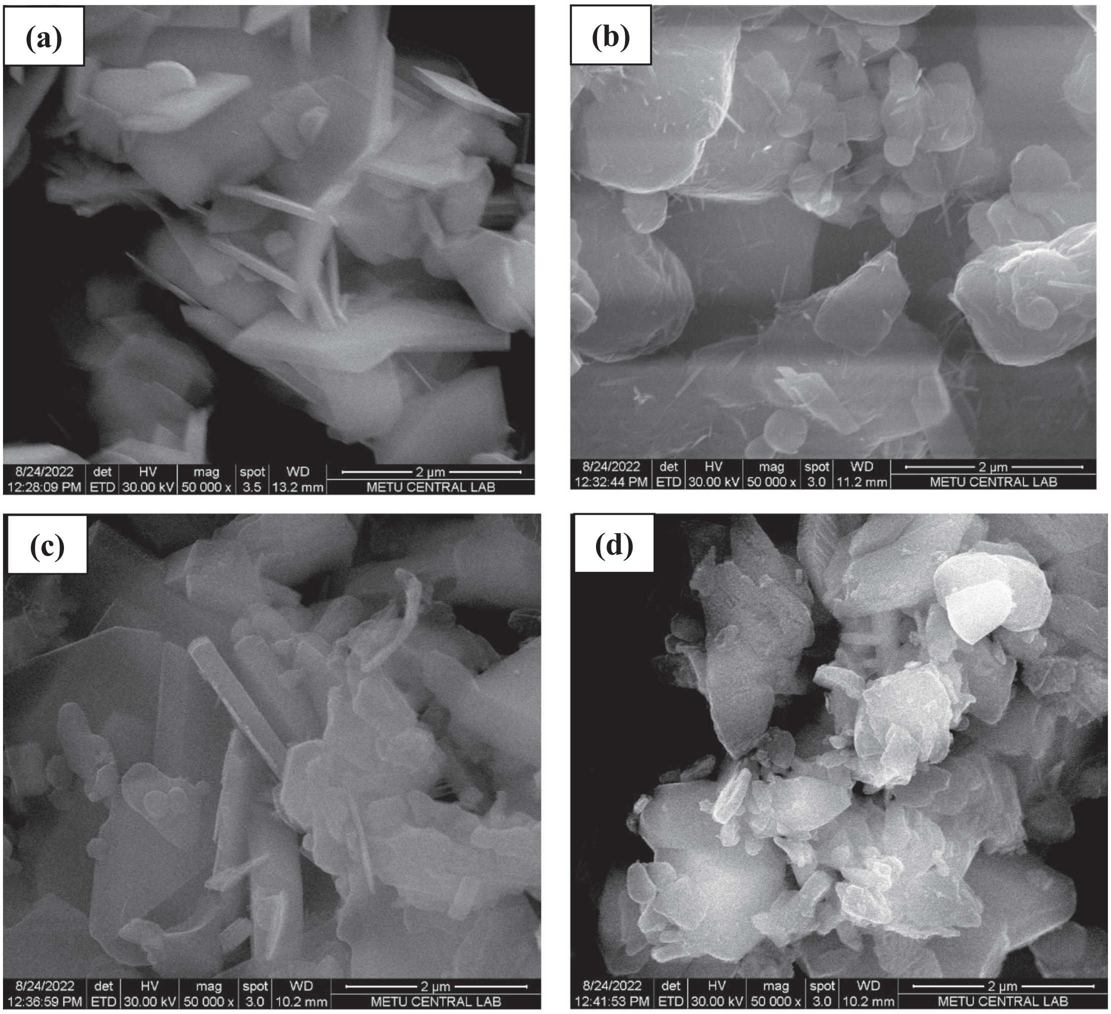

Figure 5. FESEM images of (a) pure DCP cement (b) 20% β-C_2Si/DCP, (c) 30% β-C_2Si/DCP and (d) 40% β-C_2Si/DCP cement.

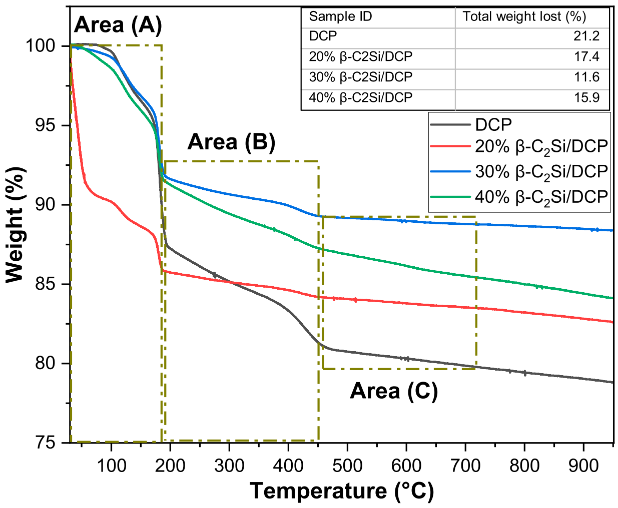

Figure 6. Thermal stability of pure DCP cement and β-C_2Si/DCP composite cement.

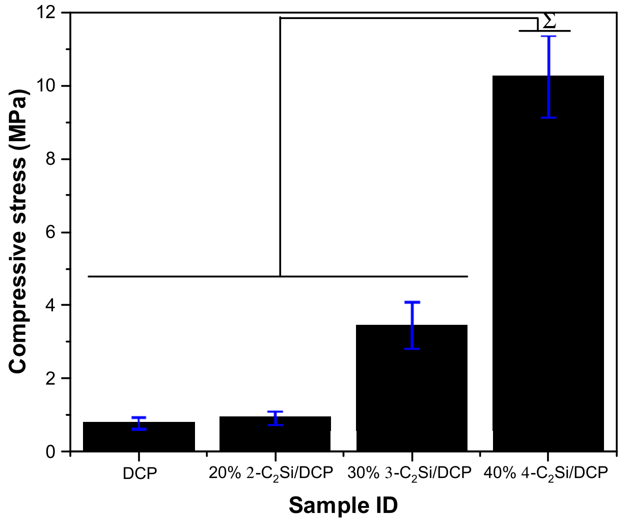

Figure 7. Compressive strengths of pure DCP and β-C_2Si/DCP cement composites. *40% β-C_2Si/DCP was significantly higher than the other group.

cement. The hydration process and the resulting products are less susceptible to thermal degradation, maintaining the structural integrity of the cement under high temperatures [14,35].

Figure 7 displays the compressive stress of the prepared cement samples. The pure DCP bone cement exhibited a compressive stress of approximately 0.78 MPa. The compressive stress for DCP is the lowest among all samples, indicating that pure DCP has the least compressive strength. Adding 20% β-C_2Si to DCP slightly increases the compressive stress compared to pure DCP, but the increase is minimal, with the compressive stress reaching approximately 0.92 MPa. This represents a small improvement in compressive strength. The compressive stress significantly increases to approximately 3.44 MPs with 30% β-C_2Si, indicating a substantial improvement in compressive stress. The 40% β-C_2Si/DCP sample shows the highest compressive stress, reaching approximately 10.22 MPa, demonstrating that increasing the β-C_2Si content further enhances the compressive stress. A clear trend shows that as the percentage of β-C_2Si in the composite increases, the compressive stress also increases. This suggests that β-C_2Si significantly contributes to the compressive strength of the composite [36]. The data suggests that incorporating β-C_2Si into DCP can enhance its mechanical properties, particularly its compressive stress. This could be beneficial for applications requiring materials with high compressive stress. When β-C_2Si hydrates, it forms calcium silicate hydrate (C–S-H) (Eq.2) [34], which significantly contributes to the mechanical strength of cement. The C–S-H produced from β-C_2Si hydration is morphologically and compositionally similar to that from other clinker phases, featuring a needle-like or fibrillar structure crucial for mechanical interlocking [37]. As the primary binding phase, C–S-H reacts with water to create a dense, cohesive microstructure, enhancing the load-bearing capacity of the cement [38,39]. Furthermore, Its mechanical properties, including tensile strength and Young's modulus, enable it to resist various stresses, thereby improving the durability and robustness of the cement [40].

$$\beta - Ca_2SiO_4 + 2H_2O \rightarrow Ca(OH)_2 + CaO{\cdot}SiO_2 \cdot H_2O \tag{2}$$

Figure 8 shows how gentamicin-loaded pure DCP cement and β-C2Si/DCP composite cements affect the growth of *S. aureus*. It shows that the amount of bacterial growth inhibition changes a lot depending on the type of cement and how much of it is used. At higher concentrations, the pure DCP cement sample demonstrates remarkable antibacterial properties, minimizing bacterial growth most effectively at a concentration of 0.2 g/mL. Several factors contribute to this superior performance: a lower degree of crystallinity in DCP cements, which leads to higher degradation rates and increased gentamicin release; a unique nanoflake-like or layered particle structure that facilitates antibiotic release; and lower mechanical properties that potentially result in higher degradation rates [41] and consequently increased drug release [42]. In contrast, the β-C_2Si/DCP composite cements show varying degrees of bacterial growth inhibition. The addition of 20% β-C_2Si exhibits the lowest antibacterials properties among all tested samples, with peak growth at 0.2 g/mL concentration (approximately 0.45 ± 0.008 abs),

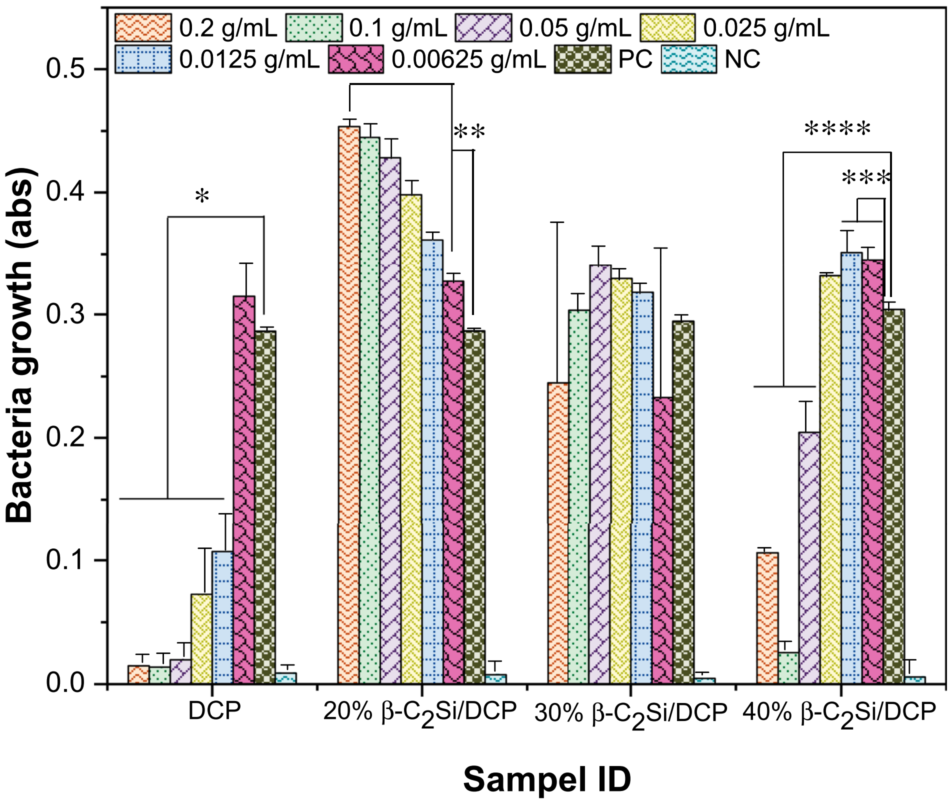

Figure 8. Effect of pure DCP and β-C_2Si/DCP composite cement loaded with gentamicin on S. aureus growth. PC: Positive Control, and NC: Negative Control. *PC was significantly higher than 0.2 g/mL, 0.1 g/mL, 0.05 g/mL, 0.025 g/mL, and 0.0125 g/mL of DCP. **PC was significantly lower than 0.2, 0.1, 0.05, 0.025, 0.0125, and 0.00625 g/mL of 20% β-C_2Si/DCP. ***PC was significantly lower than 0.0125 and 0.00625 g/mL of 40% β-C_2Si/DCP. ****PC was significantly higher than 0.2, 0.1, and 0.05 g/mL of 40% β-C_2Si/DCP.

while other concentrations also show significant bacterial growth around 0.4 abs. Incorporating 30% β-C_2Si into DCP demonstrates antibacterial properties compared to the 20% sample, with the highest growth observed at 0.05 g/mL concentration (slightly above 0.34 ± 0.016 abs), and other concentrations showing growth between 0.25 abs and 0.35 abs. The 40% β-C_2Si/DCP sample displays intermediate antibacterial properties, with the 0.0125 g/mL concentration showing the highest growth (around 0.35 ± 0.019 abs) and a significant drop in growth at the 0.1 g/mL concentration compared to the 0.2 g/mL concentration. The reduced antibacterial efficacy of β-C_2Si/DCP composites, particularly the 20% sample, may be due to lower gentamicin leaching rates, which could be attributed to the presence of silicate groups in β-C_2Si that form strong hydrogen bonds with the drug molecules, thereby reducing drug release from the cement structure. The group with the highest concentration of β-C_2Si, 40% β-C_2Si, has also shown dose-dependent antibacterial activity and achieved antibacterial activity at 0.2, 0.1, and 0.05 g/mL extract concentrations. The release of Ca and Si ions from the cement groups can further increase the antibacterial activity of Gentamicin. Previous studies also mentioned the possible contribution of Ca ion release to antibacterial activity since releasing Ca ions can raise the pH, in turn killing bacteria [43]. The study of Zhang et al. has shown that β-C_2Si cement itself can also induce an inhibition zone on *Enterococcus faecalis* (*E. faecalis)* bacteria [44].

Additionally, osmotic pressure created by released ions has been reported to contribute to antibacterial activity [21]. Calcium silicate-based materials have also been reported to develop bacteriostatic effects on various bacteria strains [45]. In this study, increasing concentrations of β-C_2Si in the cement could have contributed to antibacterial activity in the 40% β-C_2Si cement group with elevated pH and created ion concentrations.

Gentamicin demonstrates strong antibacterial efficacy against S. aureus via several potential mechanisms. Its principal mode of action targets the 30S ribosomal subunit, interfering with protein synthesis by inducing genetic code misinterpretation and halting translation. This interference results in the generation of defective, mistranslated proteins prone to misfolding and aggregation, eventually causing bacterial cell death [46]. Furthermore, gentamicin compromises the integrity of bacterial cell membranes, enhancing its bactericidal properties [47].

Figure 9 illustrates the fluorescence intensity (measured at 530/590 nm) over time (1, 4, and 7 days) for different cement compositions. The compositions tested include pure DCP cement and β-C_2Si/DCP composite cements with varying percentages (20%, 30%, and 40%) of β-C_2S, all loaded with 2 mg/mL of gentamicin. On day 1, 30% β-C_2Si/DCP composite shows the highest fluorescence intensity (Highest cell viability), while the pure DCP cement exhibits slightly lower fluorescence than pure DCP. The 20% and 40% β-C_2Si/DCP composites display similar fluorescence intensities, both higher than the control group. By day 4, all samples showed an increase in cell viability compared to day 1, with the 30% β-C_2Si/DCP composite demonstrating the highest cell viability. The 20% β-C_2Si/DCP and 40% β-C_2Si/DCP composites have no significant difference in intensities but are significantly higher than the control group. On day 7, the cell viability was significantly increased for all samples compared to Day 4. The 20% β-C_2Si/DCP composite shows the highest cell viability, while the 30% β-C_2Si/DCP and 40% β-C_2Si/DCP are higher than pure DCP. Overall, the figure demonstrates that β-C_2Si/DCP composite cements support better growth of Saos-2 cells compared to pure DCP cement, with the 20% β-C_2Si/DCP composition being the most effective in promoting cell viability.

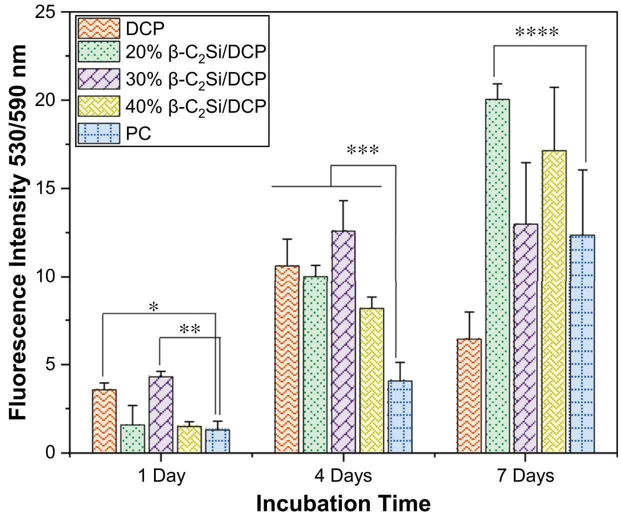

Figure 9. Effect of pure DCP cement and β-C_2Si/DCP composite cements loaded with gentamicin antibiotic on the cell viability of Saos-2 cells. *Cell growth on DCP was significantly higher than on PC. **Cell growth on 30% β-C2Si/DCP was significantly higher than on PC. ***Cell growth on all samples was significantly higher than on PC. ****Cell growth on 20% β-C2Si/DCP was significantly higher than on PC.

After 7 days of incubation, all β-C_2Si-bearing groups showed improved cell viability compared to DCP cement. The release of bioactive ions has been reported to improve both viability, proliferation, and osteogenic activity, while β-C_2Si-based cements have been shown to improve bioactivity [44]. The release of Ca and Si bioactive ions induces bioactivity and increases cell viability when bone cells interact with β-C_2Si-based cements [48]. After 7 days of incubation, bioactive ion release from all samples supported higher cell viability. As observed in various studies, the microstructural stability of β-C2Si-based cements also contributes to their

Table 2. The pH changes during the incubation period.

	Immersion Time		
Sample ID	1 d	4 Days	7 Days
DCP	6	6	6
20% β-C_2Si/DCP	8	8	8
30% β-C_2Si/DCP	7	7	7
40% β-C_2Si/DCP	8	8	8
Positive Control	8	8	8
Negative Control	8	8	8

improved bioactivity. The denser surface microstructures and the presence of biomimetic apatite remineralization on the Si-rich granule surfaces further enhance the integration with bone tissues [49].

The data suggest that pH levels significantly impact cell viability (Table 2). The pure DCP cement, with a pH of 6, supports the least cell growth. The 20% and 40% β-C_2Si/DCP composites with a pH of 8 support better cell viability than pure DCP. This indicates that a slightly alkaline environment (pH 7-8) is more conducive to Saos-2 cell growth compared to a more neutral or little acidic environment. Therefore, the pH level plays a crucial role in cell viability, with a pH of 7–8 being optimal for promoting cell proliferation in these cement compositions.

The data suggest that pH levels significantly impact cell viability. Pure DCP cement, with a pH of 6, likely supports less cell growth compared to composites with higher pH. The 20% and 40% β-C_2Si/DCP composites with a higher pH may support better cell viability than pure DCP. This indicates that a slightly alkaline environment (pH 7-8) is generally more conducive to osteoblast-like cell growth than a more acidic environment [50,51]. However, the optimal pH range for cell proliferation can vary depending on the specific cell type and culture conditions. Studies have shown that cell growth is typically optimal in a pH range of 7.38–7.87 [52,53]. Cell growth tends to decline more gradually on the acidic side of this optimal range. However, extreme acidic (pH 6.0) or alkaline (pH 9.2) conditions can retard cellular growth and induce cell death [54]. Different cell types may also respond differently to pH changes [51]. Therefore, while pH plays a crucial role in cell viability, the optimal range can vary based on specific cell types and experimental conditions.

Conclusion

This study comprehensively investigated the synthesis, characterization, and biological evaluation of β-Dicalcium Silicate (β-C_2Si) and Dicalcium Phosphate (DCP)-based cements, revealing their potential for biomedical applications. The β-C_2Si was synthesized via the sol–gel method, while β-Tricalcium Phosphate (β-TCP) was produced using microwave-assisted wet precipitation. Various β-C_2Si/DCP cement composites with different β-C_2Si contents (20%, 30%, and 40%) were formulated and analyzed. Key findings include structural and mechanical properties, antibacterial activity, cytotoxicity, and cell viability. The phase purity and structural properties of the synthesized materials were confirmed through XRD, FTIR, and FESEM analyses. The compressive strength of the composites significantly improved with increasing β-C_2Si content, with the 40% β-C_2Si/DCP composite exhibiting the highest compressive stress of approximately 10.22 MPa. *In vitro* antibacterial activity against *Staphylococcus aureus* (*S. aureus*) demonstrated that pure DCP cement loaded with gentamicin had superior antibacterial properties, particularly at a 0.2 g/mL concentration. However, the β-C_2Si/DCP composites exhibited varying degrees of bacterial growth inhibition, with the 20% β-C_2Si/DCP sample showing the lowest bacterial growth inhibition. Cytotoxicity studies using the Osteogenic sarcoma (Saos-2) cell line revealed that the β-C_2Si/DCP composites supported better cell viability compared to pure DCP cement, with the 20% β-C_2Si/DCP composition being the most effective in promoting cell growth. The optimal pH for cell proliferation was 7-8, as observed in the β-C_2Si/DCP composite. These findings suggest that β-C_2Si/DCP composites, particularly those with higher β-C_2Si content, hold promise for biomedical applications due to their enhanced mechanical properties, adequate antibacterial activity, and favourable cytocompatibility. Future research should focus on optimizing the composition and further evaluating the long-term biological performance of these composites *in vivo* to validate their potential for clinical applications.

Data availability

The datasets generated during and/or analyzed during the current study are available from the corresponding author upon reasonable request.

Disclosure statement

No potential conflict of interest was reported by the author(s).

ORCID

Ammar Z. Alshemary http://orcid.org/0000-0001-5367-1869

References

[1] Tariq U, Hussain R, Tufail K, et al. Injectable dicalcium phosphate bone cement prepared from biphasic calcium phosphate extracted from lamb bone. Mater Sci Eng C. 2019;103:109863, doi:10.1016/j.msec.2019.109863

[2] Ko C-L, Chen J-C, Tien Y-C, et al. Osteoregenerative capacities of dicalcium phosphate-rich calcium phosphate bone cement. J Biomed Mater Res A. 2015;103(1):203–210. doi:10.1002/jbm.a.35167

[3] Krüger R, Groll J. Fiber reinforced calcium phosphate cements–on the way to degradable load bearing bone substitutes? Biomaterials. 2012;33(25):5887–5900. doi:10.1016/j.biomaterials.2012.04.053

[4] Schröter L, Kaiser F, Stein S, et al. Biological and mechanical performance and degradation characteristics of

calcium phosphate cements in large animals and humans. Acta Biomater. 2020;117:1–20. doi:10.1016/j.actbio.2020.09.031

[5] Wali KJ, Saleh AT, Huseien GF. Preparation of injectable dicalcium phosphate bone cement for potential orthopedic applications. Eng. 2024;5(2):1028–1042. doi:10.3390/eng5020056

[6] Ma Y, Zhang W, Wang Z, et al. PEGylated poly (glycerol sebacate)-modified calcium phosphate scaffolds with desirable mechanical behavior and enhanced osteogenic capacity. Acta Biomater. 2016;44:110–124. doi:10.1016/j.actbio.2016.08.023

[7] Ogasawara T, Sawamura T, Maeda H, et al. Enhancing the mechanical properties of calcium phosphate cements using short-length polyhydroxyalkanoate fibers. J Ceram Soc Jpn. 2016;124(2):180–183.

[8] Motameni A, Alshemary AZ, Dalgic AD, et al. Graphene oxide reinforced doped dicalcium phosphate bone cements for bone tissue regenerations. J Aust Ceram Soc. 2022;58(5):1633–1647. doi:10.1007/s41779-022-00800-8

[9] Fada R, Shahgholi M, Karimian M. Improving the mechanical properties of strontium nitrate doped dicalcium phosphate cement nanoparticles for bone repair application. Ceram Int. 2021;47(10):14151–14159. doi:10.1016/j.ceramint.2021.02.002

[10] Ginebra M, Driessens F, Planell J. Effect of the particle size on the micro and nanostructural features of a calcium phosphate cement: a kinetic analysis. Biomaterials. 2004;25(17):3453–3462. doi:10.1016/j.biomaterials.2003.10.049

[11] Engstrand J, Persson C, Engqvist H. The effect of composition on mechanical properties of brushite cements. J Mech Behav Biomed Mater. 2014;29:81–90. doi:10.1016/j.jmbbm.2013.08.024

[12] Meininger S, Blum C, Schamel M, et al. Phytic acid as alternative setting retarder enhanced biological performance of dicalcium phosphate cement in vitro. Sci Rep. 2017;7(1):558, doi:10.1038/s41598-017-00731-6

[13] Liu Z, He X, Chen S, et al. Advances in the use of calcium silicate-based materials in bone tissue engineering. Ceram Int. 2023;49(11):19355–19363. doi:10.1016/j.ceramint.2023.03.063

[14] Correa D, Almirall A, García-Carrodeguas R, et al. Β-dicalcium silicate-based cement: synthesis, characterization and in vitro bioactivity and biocompatibility studies. J Biomed Mater Res A. 2014;102(10):3693–3703. doi:10.1002/jbm.a.35041

[15] Song X, Díaz-Cuenca A. Sol–Gel synthesis of endodontic cements: post-synthesis treatment to improve setting performance and bioactivity. Materials (Basel). 2022;15(17):6051, doi:10.3390/ma15176051

[16] Deshmukh K, Kovářík T, Křenek T, et al. Recent advances and future perspectives of sol–gel derived porous bioactive glasses: a review. RSC Adv. 2020;10(56):33782–33835. doi:10.1039/D0RA04287K

[17] Jelić A, Sekulić M, Travica M, et al. Determination of mechanical properties of epoxy composite materials reinforced with silicate nanofillers using digital image correlation (DIC). Polymers (Basel). 2022;14(6):1255, doi:10.3390/polym14061255

[18] Liu Q, Lodoso-Torrecilla I, Gunnewiek RK, et al. Tunable calcium phosphate cement formulations for predictable local release of doxycycline. Materialia. 2023;28:101769, doi:10.1016/j.mtla.2023.101769

[19] Chen L, Lin X, Wei M, et al. Hierarchical antibiotic delivery system based on calcium phosphate cement/montmorillonite-gentamicin sulfate with drug release pathways. Colloids Surf B. 2024;238:113925, doi:10.1016/j.colsurfb.2024.113925

[20] Motameni A, Dalgic AD, Alshemary AZ, et al. Structural and biological analysis of mesoporous lanthanum doped βTCP for potential use as bone graft material. Materials Today Communications. 2020;23:101151, doi:10.1016/j.mtcomm.2020.101151

[21] Yang X, Liu M, Zhao Y, et al. Rational design and fabrication of a β-dicalcium silicate-based multifunctional cement with potential for root canal filling treatment. J Mater Chem B. 2014;2(24):3830–3838. doi:10.1039/C4TB00129J

[22] Reller LB, Weinstein M, Jorgensen JH, et al. Antimicrobial susceptibility testing: a review of general principles and contemporary practices. Clin Infect Dis. 2009;49(11):1749–1755. doi:10.1086/647952

[23] Abd El-Hamid HK, Farag MM, Abdelraof M, et al. Regulation of the antibiotic elution profile from tricalcium phosphate bone cement by addition of bioactive glass. Sci Rep. 2024;14(1):2804, doi:10.1038/s41598-024-53319-2

[24] Alshemary AZ, Pazarceviren AE, Tezcaner A, et al. Mesoporous strontium doped nano sized sulphate hydroxyapatite as a novel biomaterial for bone tissue applications. RSC Adv. 2016;6(72):68058–68071. doi:10.1039/C6RA16809D

[25] Le Gars Santoni B, Niggli L, Dolder S, et al. Effect of minor amounts of β-calcium pyrophosphate and hydroxyapatite on the physico-chemical properties and osteoclastic resorption of β-tricalcium phosphate cylinders. Bioactive Materials. 2022;10:222–235. doi:10.1016/j.bioactmat.2021.09.003

[26] Terohid SAA, Heidari S, Jafari A, et al. Effect of growth time on structural, morphological and electrical properties of tungsten oxide nanowire. Appl Phys A. 2018;124:1–9. doi:10.1007/s00339-017-1423-2

[27] Alshemary AZ, Akram M, Goh Y-F, et al. Synthesis, characterization, in vitro bioactivity and antimicrobial activity of magnesium and nickel doped silicate hydroxyapatite. Ceram Int. 2015;41(9):11886–11898. doi:10.1016/j.ceramint.2015.06.003

[28] Zhu H, Guo D, Zang H, et al. Enhancement of hydroxyapatite dissolution through structure modification by krypton ion irradiation. J Mater Sci Technol. 2020;38:148–158. doi:10.1016/j.jmst.2019.03.048

[29] Makarova SV, Bulina NV, Vinokurova OB, et al. Thermal stability of iron-and silicon-substituted hydroxyapatite prepared by mechanochemical method. Powders. 2023;2(2):372–386. doi:10.3390/powders2020022

[30] Sheikh Z, Zhang YL, Grover L, et al. In vitro degradation and in vivo resorption of dicalcium phosphate cement based grafts. Acta Biomater. 2015;26:338–346. doi:10.1016/j.actbio.2015.08.031

[31] Zhou H, Yang L, Gbureck U, et al. Monetite, an important calcium phosphate compound–Its synthesis, properties and applications in orthopedics. Acta Biomater. 2021;127:41–55. doi:10.1016/j.actbio.2021.03.050

[32] Hlel F, Kamoun S, Guidara K. Investigation of phosphorus site condensation in CaHPO4 by analysis of 31P MAS-NMR tensor and X-ray powder patterns. Zeitschrift für Naturforschung A. 2006;61(7-8):375–382. doi:10.1515/zna-2006-1-202

[33] Charmforoushan A, Sorvali M, Mäkelä JM. Fast-facile synthesis of single-phase nanocrystalline β-Ca2P2O7 powder by an aerosol synthesis method. Powder Technol. 2024;434:119342, doi:10.1016/j.powtec.2023.119342

[34] Murzyn P, Malata G, Wiśniewska J, et al. Characterization of 40-year-old calcium silicate pastes by thermal

methods and other techniques. J Therm Anal Calorim. 2019;138:4271–4278. doi:10.1007/s10973-019-08519-8
[35] Yanagisawa K, Hu X, Onda A, et al. Hydration of β-dicalcium silicate at high temperatures under hydrothermal conditions. Cem Concr Res. 2006;36(5):810–816. doi:10.1016/j.cemconres.2005.12.009
[36] Abd El-Hamid H, Fayad A, Elwan R. Evaluation of bioactivity, biocompatibility, and antibacterial properties of tricalcium silicate bone cement modified with wollastonite/fluorapatite glass and glass-ceramic. Ceramics International; 2024;50(14);25322–25332.
[37] Krishnan S, Zunino F, Bishnoi S, et al. Characterisation and hydration kinetics of β-C2S synthesised with K2SO4 as dopant. Cem Concr Res. 2023;167:107119, doi:10.1016/j.cemconres.2023.107119
[38] Bach QS. Quantitative study of hydration of C3S and C2S in the reactive powder concrete together with its strength development. Appl Mech Mater. 2019;889: 294–303. doi:10.4028/www.scientific.net/AMM.889.294
[39] Liang Y. Mechanical and fracture properties of calcium silicate hydrate and calcium hydroxide composite from reactive molecular dynamics simulations. Chem Phys Lett. 2020;761:138117, doi:10.1016/j.cplett.2020.138117
[40] Hou D, Zhu Y, Lu Y, et al. Mechanical properties of calcium silicate hydrate (C–S–H) at nano-scale: A molecular dynamics study. Mater Chem Phys. 2014;146(3):503–511. doi:10.1016/j.matchemphys.2014.04.001
[41] Fosca M, Rau JV, Uskoković V. Factors influencing the drug release from calcium phosphate cements. Bioact Mater. 2022;7:341–363. doi:10.1016/j.bioactmat.2021.05.032
[42] Alge DL, Goebel WS, Chu T-MG. Effects of DCPD cement chemistry on degradation properties and cytocompatibility: comparison of MCPM/β-TCP and MCPM/HA formulations. Biomed Mater. 2013;8(2):025010, doi:10.1088/1748-6041/8/2/025010
[43] Sheethal Dsouza T, Shetty A, Dsouza N. Evaluation of pH, calcium Ion release, and dimensional stability of an experimental silver nanoparticle-incorporated calcium silicate-based cement. Bioinorg Chem Appl. 2021;2021(1):3919543.
[44] Zhang F, Yang X, Zhuang C, et al. Design and evaluation of multifunctional antibacterial ion-doped β-dicalcium silicate cements favorable for root canal sealing. RSC Adv. 2016;6(24):19707–19715. doi:10.1039/C6RA00172F
[45] Lin M-C, Chen C-C, Wu I-T, et al. Enhanced antibacterial activity of calcium silicate-based hybrid cements for bone repair. Mater Sci Eng C. 2020;110:110727, doi:10.1016/j.msec.2020.110727
[46] Krause KM, Serio AW, Kane TR, et al. Aminoglycosides: an overview. Cold Spring Harbor Perspect Med. 2016;6(6):a027029.
[47] Adaszyńska-Skwirzyńska M, Zych S, Bucław M, et al. Evaluation of the antibacterial activity of gentamicin in combination with essential oils isolated from different cultivars and morphological parts of lavender (lavandula angustifolia mill.) against selected bacterial strains. Molecules. 2023;28(15):5781, doi:10.3390/molecules28155781
[48] Agourrame H, Hnini M, Khachani N, et al. Improvement of bioactivity and investigating antibacterial properties of dicalcium silicate in an artificial saliva medium. Inorg Chem Commun. 2023;156:111191, doi:10.1016/j.inoche.2023.111191
[49] Zheng Y, Yang X, Liu S, et al. Ball milling medium may tune the self-curing property and root canal microleakage of β-dicalcium silicate-based cement. Materials (Basel). 2022;15(14):5043, doi:10.3390/ma15145043
[50] Souza A, Parnell M, Rodriguez BJ, et al. Role of pH and crosslinking ions on cell viability and metabolic activity in alginate–gelatin 3D prints. Gels. 2023;9(11):853, doi:10.3390/gels9110853
[51] Avnet S, Lemma S, Cortini M, et al. Altered pH gradient at the plasma membrane of osteosarcoma cells is a key mechanism of drug resistance. Oncotarget. 2016;7(39):63408, doi:10.18632/oncotarget.11503
[52] Mackenzie CG, Mackenzie JB, Beck P. The effect of pH on growth, protein synthesis, and lipid-rich particles of cultured mammalian cells. J Cell Biol. 1961;9(1):141–156. doi:10.1083/jcb.9.1.141
[53] Stepanovska J, Otahal M, Hanzalek K, et al. Ph modification of high-concentrated collagen bioinks as a factor affecting cell viability, mechanical properties, and printability. Gels. 2021;7(4):252, doi:10.3390/gels7040252
[54] Lee S, Shanti A. Effect of exogenous pH on cell growth of breast cancer cells. Int J Mol Sci. 2021;22(18):9910, doi:10.3390/ijms22189910